nature materials

SUPPLEMENTARY INFORMATION

DOI: 10.1038/NMAT3942

Observation of quadrupole helix chirality and its domain structure in $DyFe_3(BO_3)_4$

T. Usui, Y. Tanaka, H. Nakajima, M. Taguchi, A. Chainani, M. Oura, S. Shin, N. Katayama, H. Sawa, Y. Wakabayashi, and T. Kimura

A. X-ray absorption spectrum at Dy $M_{4,5}$ edges

We calculated the x-ray absorption spectra (XAS) ascribed to the Dy 3*d*-4*f* electric dipole (*E*1) transitions and compared them with the experimental results on $DyFe_3(BO_3)_4$. Figure 1S displays the calculated result and the spectra experimentally obtained at several temperatures between 300 K and 100 K for a single crystals of $DyFe_3(BO_3)_4$. In this temperature range, no significant change in the spectra was observed. Moreover, the experimental spectra are very similar to the calculated result. The calculations are performed for the atomic multiplet of the Dy^{3+} free ion in the paramagnetic spin state. The Slater integrals and spin-orbit coupling constants are calculated by the Hartree-Fock method with relativistic corrections. As usual, the Slater integrals are reduced to 85%. The obtained line spectra were broadened by a Gaussian for the experimental resolution and by a Lorentzian to represent the lifetime broadening. The calculated XAS spectra show a very good match with all the trivalent multiplet features, confirming that intra-atomic multiplet effects account for the observed features. Usually, the calculated XAS spectra can be separated in the three contributions formed by the dipole selection rules $\Delta J = 0, \mp 1$. In the absence of a magnetic field, however, exactly the same spectra for all three contribution with $\Delta J = 0, \mp 1$ are obtained, because of the degenerate ground state of Dy^{3+} with $J = \frac{15}{2}$ ($M = -\frac{15}{2} \sim +\frac{15}{2}$). In order to see the sensitivity of the crystal field symmetry of the ground sate to the intensity of absorption, we also performed the multiplet calculation by changing the crystal field symmetry of the ground state. The result indicates that there is no change in the total intensity of absorption. The similarity found between the calculated spectrum and the experimental ones suggests that the resonant scattering at Dy $M_{4,5}$ edges are mainly governed by the *E*1*E*1 event. Furthermore, no obvious temperature dependence is found in the spectra, indicating that the transition probability of 3*d*-4*f* *E*1 transitions is almost constant at the temperature range studied here.

DOI: 10.1038/NMAT3942

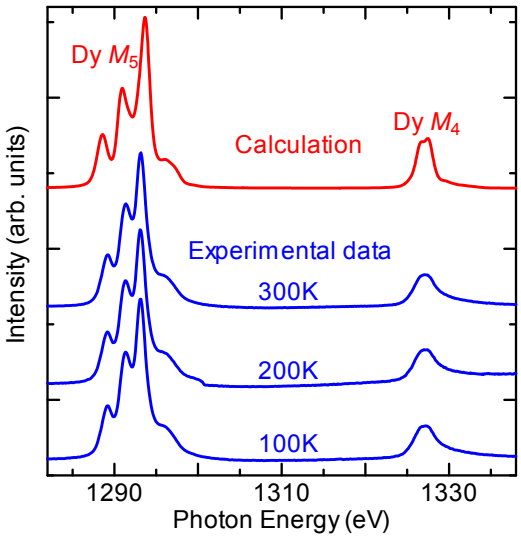

Figure S1. Comparison of Dy $M_{4,5}$ edge XAS spectra calculated for the Dy^{3+} free ion in the paramagnetic spin state (red) and experimentally obtained for a single crystal of $DyFe_3(BO_3)_4$ (blue). The experimental data were obtained via total electron yield at 300 K, 200 K, and 100 K.

B. Chiral domain image on Sample #2

Figure S2 shows a two-dimensional *yz*-scanned intensity map of forbidden reflection 001, i.e., a chiral domain structure, at 200 K for Sample #2. For the measurements, the scattering geometry was the same as illustrated in Fig. 1b in the text. The images shown in the left and the right panels of Fig. S1 were taken by using (–) and (+) helical incident x-rays, respectively. Both the images clearly show that the diffracted x-ray intensity is nearly homogeneous in all the area of the specimen. From this result, we confirm that Sample #2 consists of nearly a single chiral domain. In addition, the intensity using (–) helical x-rays is much stronger than that using (+) helical x-rays, meaning that the handedness of Sample #2 is the same as that of the region β in Sample #1 (i.e., space group: $P3_221$).

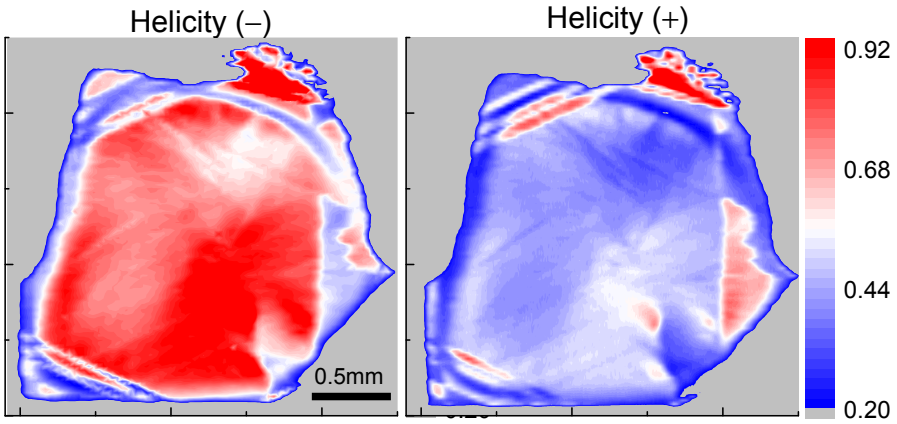

Figure S2. Chiral domain structure of Sample #2. Left and right panels show x-ray intensity maps of forbidden reflection 001 for the (–) and (+) helical incident x-rays, respectively. The data were taken at 200 K and $\Psi = 0°$

C. Crystal structure analysis

The results of the crystal structure analysis using the data obtained by single-crystal x-ray diffraction measurements are listed in Table S1, which confirms that the $DyFe_3(BO_3)_4$ crystal has the $R32$ trigonal structure at room temperature and the $P3_121$ (or $P3_221$) trigonal one below $T_s \approx 285$ K, which is consistent with previous results (refs. S1, S2). By using these structural data, we plot in Fig. S3 the temperature profiles of (a) Dy-O bond lengths and (b) the displacement of Dy position along the ξ axis from its position at 300 K ($> T_s$). The changes in the bond lengths and the displacement of Dy position toward lower T are schematically illustrated in the top panels (green and white arrows) and the middle panels (yellow arrows) in Fig. 3.

References

S1. Ritter, C., Pankrats, A., Gudim, I., & Vorotynov, A. A magnetic structure of iron borate $DyFe_3(BO_3)_4$: A neutron diffraction study. *J. Phys.: Conf. Ser.* **340**, 012065 (2012).

S2. Popova, E. A. *et al.* Magnetization and specific heat of $DyFe_3(BO_3)_4$ single crystal. *Euro. Phys. J.* B **62**, 123–128 (2008).

DOI: 10.1038/NMAT3942

Table S1. Crystallographic data, data collection, and structural refinement parameters of $DyFe_3(BO_3)_4$.

		20K	60K	100K	200K	300K
Crystal system		Trigonal	Trigonal	Trigonal	Trigonal	Trigonal
Space group		$P3_221$	$P3_221$	$P3_221$	$P3_221$	$R32$
Lattice Parameters	a (Å)	9.5266(2)	9.5280(2)	9.5298(2)	9.5337(2)	9.5425(2)
	c (Å)	7.5471(5)	7.5462(5)	7.5461(5)	7.5516(5)	7.5594(5)
	V (Å^3)	593.18(4)	593.28(4)	593.50(4)	594.42(4)	596.13(4)
Z		3	3	3	3	3
$2\theta_{max}$		119.74	119.76	119.76	115.40	113.02
No. of unique reflections used		3882	3742	2742	1794	635
No. of variables		95	95	95	95	35
Residuals: R [$I > 2.00\sigma(I)$]		0.0238	0.0236	0.0227	0.0192	0.0185
Residuals: R_w [$I > 2.00\sigma(I)$]		0.0611	0.0614	0.0581	0.0502	0.0480
Goodness of fit indicator		1.032	1.037	1.051	1.052	1.087

Table S2. Atomic coordinates of $DyFe_3(BO_3)_4$ at several temperatures.

Site		20K	60K	100K	200K	300K		Site
Dy	x	0.665037(6)	0.665218(6)	0.665464(6)	0.666029(6)	0	x	Dy
(3a)	y	0	0	0	0	0	y	(3a)
	z	2/3	2/3	2/3	2/3	0	z	
	U_{Iso}	0.00154(1)	0.00199(1)	0.00257(3)	0.00444(4)	0.00703(6)	U_{Iso}	
Fe(1)	x	0.11556(3)	0.11540(3)	0.11544(4)	0.11559(6)	0.11711(7)	x	Fe(1)
(3a)	y	0	0	0	0	1/3	y	(9d)
	z	2/3	2/3	2/3	2/3	1/3	z	
	U_{Iso}	0.00181(3)	0.00198(3)	0.00221(4)	0.00326(5)	0.00496(10)	U_{Iso}	
Fe(2)	x	0.45123(3)	0.45102(3)	0.45094(4)	0.45076(6)			
(6c)	y	0.663954(16	0.664006(16	0.664093(18	0.664423(19			
	z	0.32281(2)	0.32303(2)	0.32333(2)	0.32469(2)			
	U_{Iso}	0.00187(2)	0.00205(2)	0.00226(4)	0.00339(5)			
O(1)	x	0.07765(11)	0.07785(11)	0.07772(14)	0.07736(16)	1/3	x	O(1)
(3b)	y	0	0	0	0	-0.1886(3)	y	(9e)
	z	1/6	1/6	1/6	1/6	1/6	z	
	U_{Iso}	0.00423(13)	0.00461(14)	0.00545(19)	0.0076(2)	0.0066(4)	U_{Iso}	

O(2)	x	0.69301(10)	0.69237(10)	0.69148(12)	0.68832(13)	1/3	x	O(2)
(6*c*)	y	0.41772(10)	0.41771(10)	0.41736(13)	0.41631(14)	0.0747(5)	y	(9*e*)
	z	0.20366(10)	0.20278(10)	0.20160(12)	0.19698(12)	1/6	z	
	U_{Iso}	0.00448(9)	0.00468(9)	0.00559(12)	0.00801(14)	0.0121(6)	U_{Iso}	
O(3)	x	0.12144(14)	0.12118(14)	0.12100(18)	0.1211(2)	0.1863(3)	x	O(3)
(6*c*)	y	0.30421(13)	0.30414(13)	0.30445(18)	0.3048(2)	0.2111(3)	y	(18*f*)
	z	0.17883(13)	0.17880(13)	0.17894(14)	0.17967(16)	0.1823(2)	z	
	U_{Iso}	0.00399(11)	0.00422(11)	0.00450(16)	0.0060(2)	0.0087(3)	U_{Iso}	
O(4)	x	0.36251(13)	0.36256(13)	0.36228(17)	0.3619(2)			
(6*c*)	y	0.14755(14)	0.14758(14)	0.14731(18)	0.1477(2)			
	z	0.18581(13)	0.18549(13)	0.18526(14)	0.18485(16)			
	U_{Iso}	0.00382(10)	0.00403(11)	0.00418(16)	0.00582(19)			
O(5)	x	0.67003(8)	0.66992(8)	0.66988(9)	0.66959(10)			
(6*c*)	y	0.14517(16)	0.14502(16)	0.1455(2)	0.1453(3)			
	z	0.17536(11)	0.17516(10)	0.17499(12)	0.17386(10)			
	U_{Iso}	0.00333(12)	0.00350(12)	0.0038(2)	0.0051(3)			
O(6)	x	0.81236(17)	0.81227(17)	0.8127(2)	0.8125(3)			
(3*b*)	y	0	0	0	0			
	z	1/6	1/6	1/6	1/6			
	U_{Iso}	0.00344(15)	0.00356(15)	0.0036(2)	0.0051(3)			
O(7)	x	0.52421(14)	0.52401(14)	0.52383(18)	0.5228(2)			
(6*c*)	y	0.53501(14)	0.53528(14)	0.53567(18)	0.5366(2)			
	z	0.18595(13)	0.18570(13)	0.18556(14)	0.18515(16)			
	U_{Iso}	0.00387(11)	0.00415(11)	0.00432(16)	0.0060(2)			
B(1)	x	0.66815(14)	0.66816(14)	0.66810(17)	0.66805(18)	1/3	x	B(1)
(3*b*)	y	0	0	0	0	2/3	y	(3*b*)
	z	1/6	1/6	1/6	1/6	1/6	z	
	U_{Iso}	0.0037(3)	0.0036(3)	0.0044(5)	0.0055(6)	0.0061(8)	U_{Iso}	
B(2)	x	0.67551(14)	0.67527(14)	0.67480(15)	0.67370(16)	1/3	x	B(2)
(6*c*)	y	0.5517(2)	0.5520(2)	0.5521(3)	0.5522(3)	0.2184(4)	y	(9*e*)
	z	0.18060(17)	0.18014(17)	0.17972(19)	0.17807(15)	1/6	z	
	U_{Iso}	0.00349(16)	0.00356(16)	0.0037(2)	0.0049(3)	0.0055(4)	U_{Iso}	
B(3)	x	0.2220(2)	0.2221(2)	0.2221(3)	0.2218(3)			
(3*b*)	y	0	0	0	0			
	z	1/6	1/6	1/6	1/6			
	U_{Iso}	0.0036(2)	0.0034(2)	0.0033(3)	0.0045(3)			
Site		20K	60K	100K	200K	300K		Site

DOI: 10.1038/NMAT3942

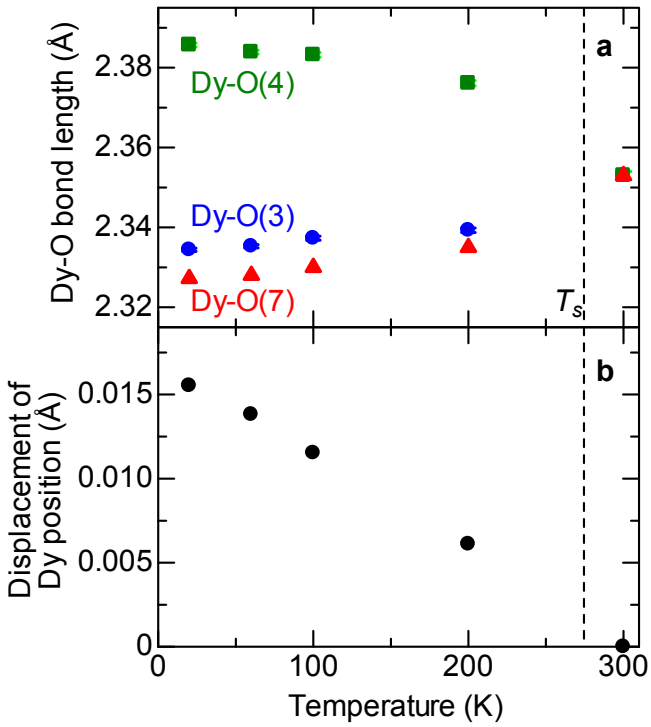

Fig. S3. Temperature profiles of (a) Dy-O bond lengths and (b) the displacement of Dy position along the ξ axis from its position at 300 K (> T_s).